

## The influence of spatial patterns in rainfall on shallow landslides

Hugh G. Smith <sup>a,\*</sup>, Andrew J. Neverman <sup>a</sup>, Harley Betts <sup>a</sup>, Raphael Spiekermann <sup>b</sup>

<sup>a</sup> Manaaki Whenua – Landcare Research, Palmerston North, New Zealand

<sup>b</sup> GeoSphere Austria, Vienna, Austria

### ARTICLE INFO

#### Keywords:

Landslide susceptibility

Shallow landslides

Weather radar

New Zealand

### ABSTRACT

Understanding how rainfall events influence the pattern and magnitude of landslide response is an important research focus from geomorphological and hazard planning perspectives. Few studies quantitatively relate spatial patterns in rainfall and landslides, largely due to difficulties in acquiring landslide inventories and data on rainfall patterns for individual storm events. However, the increasing availability of frequent, high-resolution satellite imagery and weather radar is overcoming these impediments. Here, we aim to a) identify which factors most influence susceptibility to shallow landslides at the event scale and b) assess how the spatial density of landslides varies in relation to rainfall. We combine landslide inventories spanning study areas located across the upper North Island of New Zealand with rainfall estimates from weather radar to assess the influence of different explanatory variables using a logistic regression model. We found land cover and slope exert the largest influence on landslide susceptibility ahead of intra-event rainfall intensities and pre-event rainfall accumulations. Of the rainfall variables, maximum 12-h rainfall normalised by the 10-y recurrence interval intensity and the 10-d pre-event accumulation normalised by mean annual rainfall had the most influence on susceptibility. Forest cover reduced the sensitivity of landslide spatial density to variations in slope, rainfall, and rock type, in contrast to pasture. We observed a 3.5-fold increase in mean landslide density once the maximum 12-h intensity was  $\geq 25\%$  above the 10-y recurrence interval intensity for pastoral land on weak sedimentary rocks. This threshold is consistent with the increase in 12-h rainfall by late century under the highest levels of projected warming in New Zealand, which suggests that the landslide response to storm rainfall could be significantly amplified by climate change. Our study demonstrates the insights gained from combining event inventories with spatial rainfall data to better understand factors influencing landslide susceptibility.

### 1. Introduction

High-magnitude rainfall events trigger large numbers of landslides each year globally causing loss of life, significant socio-economic costs, and environmental impacts (Petley, 2012; Bowman, 2022). Understanding how rainfall events influence the pattern and magnitude of landslide response is therefore an important focus for research from geomorphological and hazard planning perspectives (Marc et al., 2018; Emberson et al., 2022). Many studies investigate factors influencing rainfall-induced landslide occurrence using statistical or machine-learning approaches to model landslide susceptibility. These studies tend to focus on geo-environmental factors such as slope, land cover, and rock type (Reichenbach et al., 2018), and do not generally consider the influence of rainfall when assessing susceptibility (Steger et al., 2023). Even fewer studies attempt to quantitatively relate spatial patterns in rainfall and landslide response for individual storm events (Marc

et al., 2019).

Most studies of landslide susceptibility employ geomorphological or multi-temporal landslide inventories (Reichenbach et al., 2018). These inventories generally reduce the influence of spatial patterns in rainfall associated with individual events on susceptibility models. While such event-scale rainfall patterns can be problematic when modelling susceptibility based on geo-environmental variables alone, the inclusion of spatial rainfall data presents an opportunity to better understand how landslide occurrence varies in relation to both rainfall and landscape-based factors. For example, it has been postulated that large rainfall gradients within high-magnitude storm events may produce spatial landslide responses that deviate from conventional susceptibility models as the importance of different slope stability factors vary with zones defined by rainfall intensity (Crozier, 2017).

Past impediments to the analysis of rainfall-induced landslide events include difficulties in acquiring event-specific landslide inventories and

\* Corresponding author.

E-mail address: [smith@landcareresearch.co.nz](mailto:smith@landcareresearch.co.nz) (H.G. Smith).

limited information on spatial rainfall patterns at adequate resolution. The increasing availability of frequent, high-resolution satellite imagery better enables before/after bracketing of events and the attribution of mapped landslides to triggering rainfall (Guzzetti et al., 2012; Smith et al., 2021). Combining event landslide inventories with spatial rainfall information opens new research opportunities but requires high-resolution spatio-temporal data. The sparsity of most rain gauge networks remains an important impediment to event analysis, particularly in mountainous areas (Chiang and Chang, 2009). Spatial interpolation of daily rainfall has been used to produce gridded inputs for modelling (Lin et al., 2022; Steger et al., 2023) but these approaches are less suited to areas with few gauges, while the daily timestep misses shorter duration, intense rainfall that may initiate landslides (Leonarduzzi et al., 2017).

Ground-based weather radar provides an alternative technique for estimating rainfall. Radar-derived estimates can achieve spatial ( $\leq 1 \text{ km}^2$ ) and temporal ( $< 60 \text{ min}$ ) resolutions that tend to be better suited for modelling rainfall-induced landslides (Chiang and Chang, 2009; Berenguer et al., 2015). Rainfall depths converted from radar reflectivity may be bias corrected with gauge data to provide quantitative precipitation estimates (QPEs) with accompanying error statistics. Such spatio-temporal rainfall estimates have been used to assess event-scale spatial patterns in landslides (Marc et al., 2019), derive threshold-exceeding event frequencies for landslide susceptibility modelling (Tseng et al., 2020), and may form the basis for early-warning systems (Berenguer et al., 2015).

In the present study, we aim to better understand the relationship between storm event rainfall and the shallow landslide response. We focus on intra-event rainfall magnitude-intensities as well as pre-event rainfall that may have a preparatory effect on landslide occurrence (Knevels et al., 2020; Steger et al., 2023) in combination with geo-environmental factors. Our study seeks to a) identify which factors most influence susceptibility to shallow landslides and b) assess how the spatial density of landslides varies in relation to rainfall. We adopt a statistical modelling approach to assess the influence of different explanatory variables at the event scale. While we do not know precisely when individual landslides were triggered during an event, we can examine how the overall pattern of landslides varies spatially in relation to rainfall and geo-environmental factors.

We use an inventory comprising over 26,000 shallow landslides spanning four study areas located across the upper North Island of New Zealand. Most landslides in New Zealand are rapid shallow slides and flows that occur in regolith in response to high magnitude rainfall events (Crozier, 1996; Basher, 2013; Fig. 1). In the present study, we focus on



**Fig. 1.** Typical shallow landslides located on pastoral hill country terrain on the North Island of New Zealand (location not within present study areas) (photo Harley Betts).

areas that include extensive hill country terrain (defined as land  $< 1000 \text{ m}$  in elevation with slopes generally between 20 and 30°) where rainfall-induced rapid landslides are typically shallow (approximately 1 m deep) and small (median source areas 50–100 m<sup>2</sup>) (Crozier, 1996; Betts et al., 2017; Smith et al., 2021).

Past land clearing accelerated landslide erosion in New Zealand (Trustrum et al., 1999; Basher, 2013). Storm events trigger hundreds to thousands of these shallow landslides (Smith et al., 2021) causing significant erosion damage to land, infrastructure, and culturally significant sites, as well as agricultural production losses and degradation of receiving environments from excess sediment (Krausse et al., 2001; Dominati et al., 2014). To reduce these impacts, better understanding of the factors that determine where landslides are likely to occur is needed to improve targeting of erosion control measures (Phillips et al., 2021). We also require information on rainfall magnitude-frequency in relation to landslide impacts to support hazard planning.

## 2. Methods

### 2.1. Study areas

Study areas were selected based on reports of rainfall-triggered landslides, the availability of mostly cloud-free, intersecting pre- and post-storm very high resolution (VHR,  $\leq 0.5 \text{ m}$  resolution) satellite imagery, and ground-based weather radar coverage. The use of VHR imagery is necessary for accurate mapping of shallow landslide source areas given the typical size (50–100 m<sup>2</sup>) of these features (Smith et al., 2021; Spiekermann et al., 2022). The imagery selected (Table 1) represents the best available within the shortest interval before the date of the landslide triggering storm, while post-event imagery was available 1–7 months after triggering events.

The four study areas are located across the upper North Island of New Zealand (Fig. 2) and range in size from 178 to 401 km<sup>2</sup>. The Whanganui and Coromandel study areas are represented by two discrete areas of interest (Fig. 2). Within the constraints imposed by image availability, study area delineation focused on representing gradients in storm event rainfall that span areas most impacted by landslides through to areas that experienced rainfall but little or no landslide response. Two of the study areas, namely Whanganui (west) and Waikato (Fig. 2), formed part of earlier work (Smith et al., 2021). These two areas of interest (AOI) were targeted to the areas most impacted by landslides. Subsequently, the Whanganui study area was extended through the addition of a second 291 km<sup>2</sup> AOI to the east that spans a larger range in storm rainfall and landslide impact. The Hunua Ranges and Coromandel (north and south) study areas were identified based on local reports and included for analysis (Table 1).

The Whanganui and Wairarapa study areas contain mostly hill country terrain underlain by a range of Tertiary and Quaternary sedimentary rocks, which in the Whanganui study area are overlain by volcanic ash pre-dating the Taupo eruption c. 1820 years ago (Fig. 3). Greywacke is the dominant rock type across the Hunua Ranges study area, whereas volcanic rocks and ash beds dominate the Coromandel areas (Table 1; Fig. 3). Land cover comprises a mix of pasture, native forest and scrub, and exotic pine plantations, including areas harvested prior to the storm events. Land cover was determined from the NZ Land Cover Database (LCDB v5.0, 2018) which is based on thematic classification of satellite imagery. Pre-event imagery was used to re-map areas classed as plantation forest in the LCDB where harvesting had occurred just prior to the storm event. Recently harvested areas were identified from the change in land cover and were predominantly characterised by bare ground.

### 2.2. Rainfall events

Storm rainfall data is available from rain gauges located within or near the study areas (Table 1). While the individual storms that

**Table 1**  
Summary information for study areas.

Location <sup>1</sup>	Area (km <sup>2</sup> )	Storm period	Event rainfall <sup>2</sup> (mm) and [duration, hours]	ARI <sup>3</sup> (y) and [duration, hours]	Dominant rock types	Imagery sources pre- and post-event (resolution)
Whanganui [W and E]	401	7–8 March 2018	82–165 [24] 85–177 [48]	2–250 [24] 1.58–80 [48]	Volcanic ash beds (62 %), mudstone (15 %), sandstone (12 %)	Pre: Pleiades-1A Post: Worldview-2 (0.5 m)
Wairamarama, Waikato	178	4–5 April 2017	127 [24] 138 [48]	10–20 [24] 10 [48]	Mudstone (41 %), sandstone (40 %), argillite (8 %)	Pre: Pleiades-1A Post: GeoEye-1 (0.5 m)
Hunua Ranges, Auckland	283	7–8 March 2017	181–240 [24] 184–251 [48]	60–250 [24] 30–100 [48]	Greywacke (67 %), sandstone (8 %), volcanic ash beds (8 %)	Pre: Pleiades-1A Post: GeoEye-1 (0.5 m)
Coromandel, Waikato [N and S]	255	7–11 March 2017	86–412 [24] 135–536 [48] 226–824 [120]	<1.58–20 [24] <1.58–20 [48] 2–30 [120]	Volcanic rocks (60 %), volcanic ash beds (25 %), greywacke (6 %)	Pre: Pleiades-1A and Worldview-2 Post: Worldview-2 and Worldview-3 (0.5 m)

<sup>1</sup> Whanganui and Coromandel comprise discrete east (E)/west (W) and north (N)/south (S) study areas, respectively.

<sup>2</sup> Rainfall recorded at gauges located within or near the AOIs and intensity-durations calculated from hourly records in UTC.

<sup>3</sup> Average recurrence intervals (ARI) obtained for rain gauge locations from NIWA's High Intensity Rainfall Design System (HIRDS) v4.

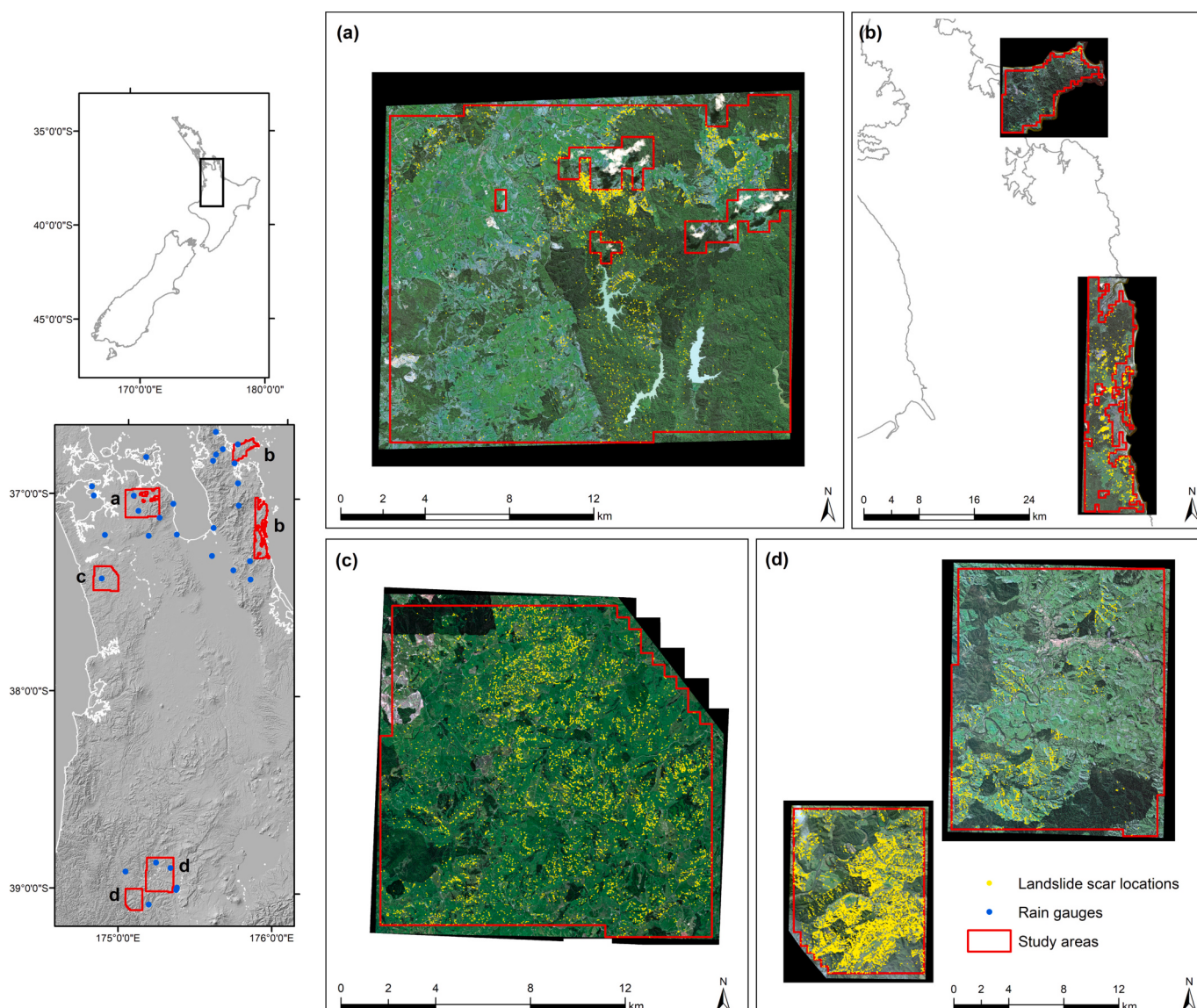


**Fig. 2.** Locations of the four study areas comprising a) Hunua Ranges, b) Coromandel, c) Wairamarama, and d) Whanganui showing mapping extents, rain gauge, and shallow landslide locations.

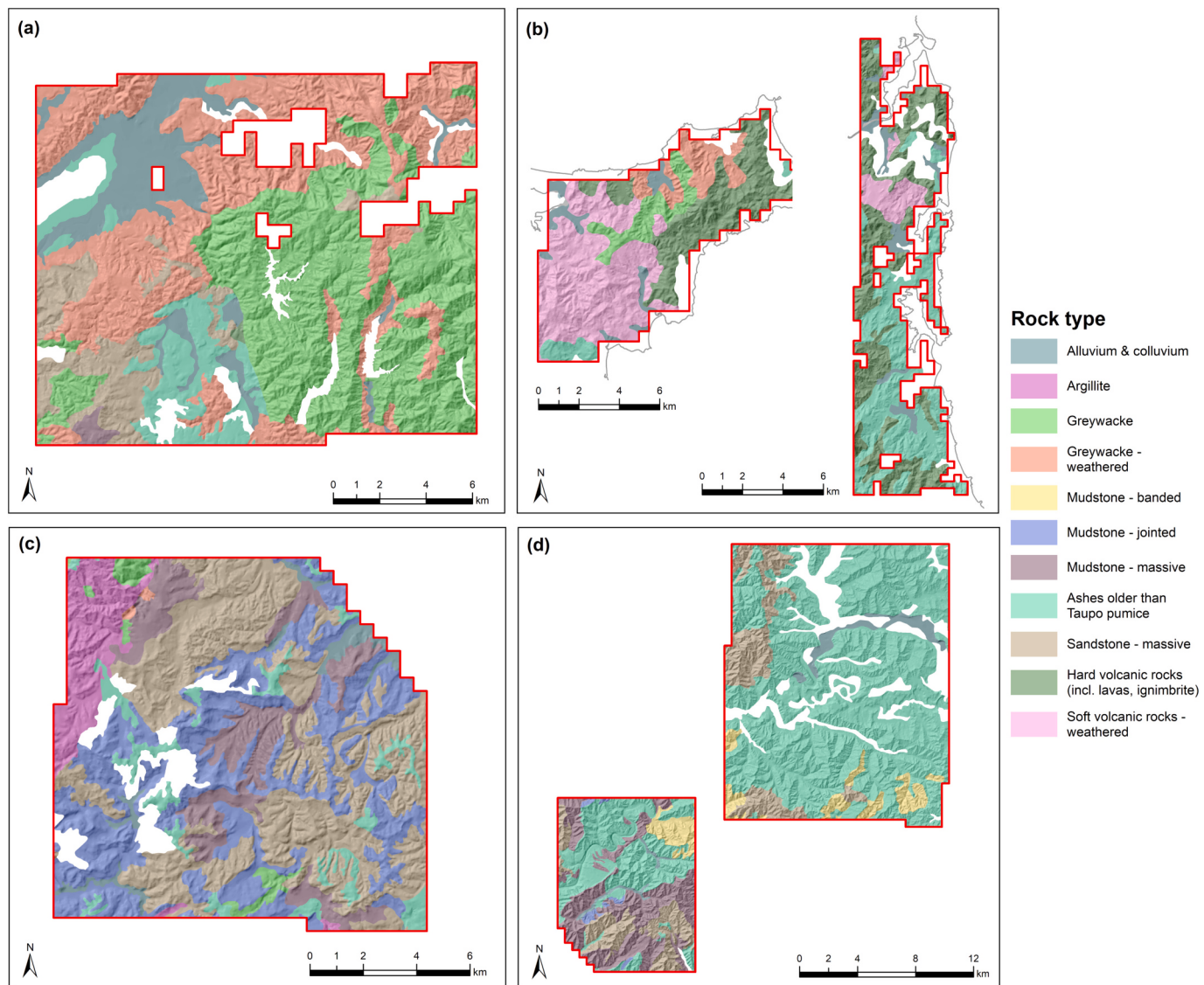


**Fig. 3.** Rock types present within each study area. Rock types with insufficient landslide/non-landslide data for inclusion in statistical modelling or non-landslide producing areas (e.g., lakes) are shown as white polygons within the red study area boundaries. (For interpretation of the references to colour in this figure legend, the reader is referred to the web version of this article.)

triggered the main landslide response have been confirmed, there is the potential for limited occurrence of new landslides in the period between the main triggering event and post-event imagery capture. However, there were no reports of subsequent landslide-triggering events. Large variations in event rainfall were recorded across those study areas with multiple gauges (Table 1).

Whanganui storm event rainfall amounted to 85–177 mm in 48 h in March 2018 based on rain gauges located either inside or within 3.5 km of the boundary of the two mapping areas. Most of the rainfall occurred within 24 h (82–165 mm). Rainfall was highest in the south-west and declined to the north, which produced a large range in the estimated average recurrence interval (ARI), spanning 1.58 to 80 y over 48 h. The Wairamarama event in April 2017 experienced the lowest rainfall total of the four event study areas with 138 mm in 48 h (10 y ARI) measured at a gauge near the centre of the study area. No other rain gauges were available within the vicinity of this study area.

Rainfall over the Hunua Ranges study area formed part of a longer duration event that also affected the Coromandel study area. Local reports indicated that the landslides affecting the Hunua Ranges study area occurred in response to rainfall over 7–8 March 2017. Rainfall

across this study area ranged 184–251 mm over 48 h (30–100 y ARI) based on gauges located inside or within 1 km of the study area boundary. Most of the rainfall occurred within 24 h (181–240 mm with 60–250 y ARI).

The longer duration Coromandel storm event (7–11 March 2017) ranged 135–536 mm and 226–824 mm over 48 and 120 h, respectively. These rainfall totals equate to <1.58–20 and 2–30 y ARIs, respectively, based on gauges located within 10 km of the two Coromandel study areas. The contrast in rainfall and corresponding ARIs between the Hunua Ranges and Coromandel study areas reflect differences in climate, with higher mean annual rainfall over the Coromandel peninsula compared to areas on the western side of the Hunua Ranges.

### 2.3. Weather radar

Ground-based weather radar data is available across New Zealand from a network of scanning C-Band doppler radars operated by the Meteorological Service of New Zealand Ltd. (MetService). The closest radar to each study area was used to estimate spatial patterns in intra- and pre-event rainfall. Data from the New Plymouth radar was used for

the Whanganui study area, and the Auckland radar was used for the Hunua Ranges, Coromandel, and Wairamarama study areas. We use reflectivity data from the lowest angle scans ( $0.5^\circ$  elevation), performed on a 7.5 min cycle, to estimate rainfall depth over a  $1 \times 1$  km grid. Reflectivity values (Z) were converted to rainfall (R) using the Marshall-Palmer Z-R relationship,  $Z = 200R^{1.6}$ , to calculate rainfall depth for each 7.5 min scan window, and subsequently bias corrected with rain gauge data.

As rain gauge data were limited to daily totals, we bias correct the radar estimates at daily timesteps to derive a multiplicative bias field which is used for temporal downscaling to correct the individual 7.5 min radar scans, following Cecinati et al. (2017). This method provides a balance between reduced error in rainfall totals, while preserving temporal variability in intensity. For pre-event rainfall estimates, we derive bias fields for monthly accumulations and apply these to daily radar-derived rainfall depth grids. This was done to overcome limitations with applying higher temporal resolution bias corrections to rainfall records with days of low or no rainfall.

The availability of rain gauge data for bias correction varied between study areas. The Wairamarama study area contains one rain gauge, with few other gauges close enough for inclusion. Therefore, a uniform bias correction was applied using the single gauge located near the centre of the study area. In contrast, six gauges are located within the Whanganui study areas, 10 within and near the Hunua Ranges study area, and 13 within and near the Coromandel study areas (Fig. 2). At each rain gauge location, the gauge observation was compared with the estimated rainfall depth in the overlying radar grid pixel to derive a multiplicative bias correction factor.

Ordinary Kriging is commonly used for bias correction and has been shown to be the best performing univariate method (Nanding et al., 2015), thus it was used to derive a gridded bias field for the three remaining study areas. Ordinary kriging considers the spatial variability of observations, deriving a local rather than global function (Serrano-Notivoli and Tejedor, 2021), allowing it to capture spatial variability in the bias field. Due to the low number of gauges proximal to each study area, and the need to use all gauges to capture the spatial variation in the bias field, excluding some gauges for independent validation is unfeasible (Ochoa-Rodriguez et al., 2019). Given Ordinary Kriging does not use the exact values from observation points within the outputs, comparison between bias-adjusted radar pixel values and rain gauge observations can be used to assess fit. We calculated the root mean square error (RMSE) between gauge observations and radar estimates at each gauge. As a measure of fit, the RMSE for events ranged 0.2–6.7 mm compared to daily rainfall of 0–412 mm (mean 79 mm) recorded at the gauges used for bias correction. For pre-event rainfall, RMSEs ranged 0.9–8.8 mm compared to monthly rainfall of 13–243 mm (mean 96 mm) recorded at gauges over a 3-month period prior to the storm events.

#### 2.4. Landslide mapping

Landslide mapping adopted a manual approach that involved placing a single point at the centre of individual landslide source areas (scars) (cf. Petschko et al., 2015; Smith et al., 2021). Shallow landslide scars were identified in pre- and post-event imagery for each AOI, and pre-existing scars were excluded from subsequent analysis. The size of study areas and the large number of scars present meant it was not practical to manually delineate scar areas. The total number of landslide scars mapped with points equated to 26,558 across the four study areas. The landslide counts within the Whanganui, Wairamarama, Hunua Ranges, and Coromandel study areas were 13,441, 7704, 4024, and 1389, respectively.

The use of point-based mapping is appropriate given the small size of shallow landslide scars across the study areas. Previous landslide scar area mapping that included the Wairamarama study area and the southern Whanganui area found the median scar size ranged 50–106 m<sup>2</sup> (Smith et al., 2021). Moreover, the use of a single point to represent each

individual scar instead of polygons that may cover multiple raster grid cells reduces the spatial autocorrelation between observations (Petschko et al., 2014; Goetz et al., 2015). In the present study, a single DEM grid cell (225 m<sup>2</sup>) encompasses a typical landslide scar. Additionally, Petschko et al. (2013) found that the choice of point location within a landslide scar had little effect on statistical landslide susceptibility analysis.

#### 2.5. Explanatory variables

Potential explanatory variables were assembled from nationally available datasets following Smith et al. (2021). These comprise elevation (15 m digital elevation model), rock type (mapped 1:63,360 scale with some areas subsequently remapped at 1:50,000 scale (NZ Land Resources Inventory, NZ LRI, Newsome et al., 2008), and land cover from thematic classification of satellite imagery (NZ Land Cover Database, LCDB v5.0, from 2018 with a minimum mapping area of 1 ha). Slope angle, flow accumulation, aspect, and curvature were derived from the DEM.

These variables were selected given a) the potential physical basis for influencing landslide occurrence and b) data availability across all study areas. Slope is a fundamental physical control on landslide susceptibility. Topographic form (i.e., aspect, curvature, upslope contributing area) may influence patterns of soil moisture and soil development that could affect susceptibility (Burnett et al., 2008; Catani et al., 2013; Crozier, 2017). Slopes were partitioned based on planform (i.e., perpendicular to the direction of maximum slope, classified as convergent/divergent/flat) and profile (i.e., parallel to the direction of maximum slope, classified as convex/concave/flat) curvature (Catani et al., 2013). Land cover is used as a proxy for the effects of tree root reinforcement and alterations in soil moisture (Phillips and Marden, 2005; Stokes et al., 2014). Rock type may indirectly influence landslide susceptibility via regolith properties and slope angle rather than directly via bedrock strength given shallow landslides (typically 1 m deep) in New Zealand generally occur in regolith (Crozier, 1996; Crozier et al., 1980; Reid and Page, 2002; Betts et al., 2017).

Rainfall explanatory variables were derived for intra-event, total event, and pre-event rainfall accumulations. Maximum intra-event intensities (mm h<sup>-1</sup>) were computed from the bias corrected radar grids (1 km resolution) for a range of durations comprising 30 min, 60 min, 2 h, 6 h, 12 h, and 24 h across all study areas (Fig. 4). We did not compute a maximum intensity over 48 h as this corresponds to the total event rainfall for three of the four study areas. Landslides may be triggered by intense rainfall over short intervals as well as accumulations over longer durations (Iverson, 2000). Hence, we focus on a range of maximum intensities in addition to the total event rainfall to assess the influence of spatial patterns in intra-event rainfall on landslide occurrence.

Pre-event rainfall accumulations were computed from bias corrected daily radar grids over 10, 30, 60, and 90 d durations. Pre-event rainfall accumulation can be used as a proxy for antecedent soil moisture (Guzzetti et al., 2007). Higher antecedent moisture increases the likelihood that rainfall during an event produces positive porewater pressures and slope failure (Crozier, 1999; Rahimi et al., 2011). The focus on a 10–90 d range in pre-event rainfall reflects atmospheric-driven temporal variations in soil moisture that occur over larger areas on seasonal timescales of 2–3 months for the top 1-m soil layer (Entin et al., 2000; Wilson et al., 2004). This soil depth corresponds closely to measured depths (mean 0.7–1.0 m) of shallow landslide scars in New Zealand's hill country (Betts et al., 2017). In contrast, shorter-term and more localised patterns in soil moisture are related to variations in discrete events and land surface characteristics affecting infiltration and drainage (Entin et al., 2000).

Maximum intra-event intensities were normalised by rainfall intensities corresponding to the estimated 10-year recurrence interval for each duration (Fig. 4) based on the High Intensity Rainfall Design System (HIRDS v4) (Carey-Smith et al., 2018). The HIRDS v4 data are

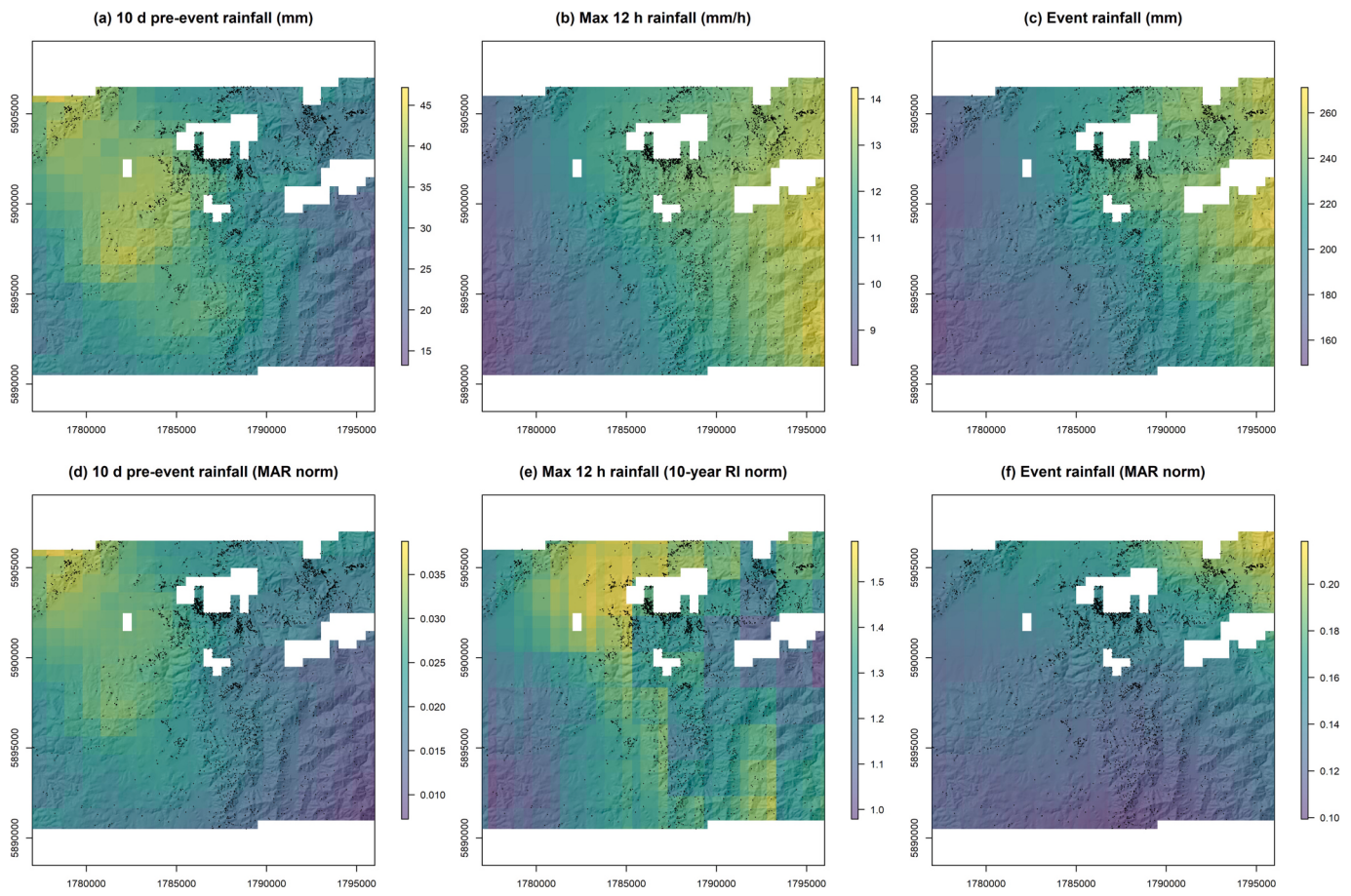


**Fig. 4.** Examples of quantitative precipitation estimates (1 km) from radar for a) 10-day pre-event accumulation, b) maximum 12 h intensity, c) total event rainfall and the corresponding normalised grids for d) pre-event normalised by mean annual rainfall (MAR) on a 500 m grid, e) 12 h intensity normalised by the 10-year recurrence interval (RI) intensity on a 2 km grid, and f) event rainfall normalised by MAR. Black points give the location of mapped landslides. Gaps in the data indicate areas with cloud cover in the post-event satellite imagery that were not mapped.

available nationally at a 2 km grid resolution. The 10-year recurrence interval was selected as the minimum recurrence interval corresponding to the maximum rainfall intensities recorded over 24 h at rain gauges within or near the study areas. Total event and pre-event (10–90 d) rainfall accumulations were normalised by mean annual rainfall (1981–2010) available at 500 m grid resolution. Normalisation of rainfall data reflects coevolution of soils and hillslopes with climate whereby landscapes adjust to repeated landsliding (Marc et al., 2019), which may produce contrasts in rainfall thresholds for landslide initiation (Guzzetti et al., 2008). Normalisation therefore better enables comparison between study areas that vary climatically.

Statistical modelling requires data corresponding to landslide and non-landslide point locations for all explanatory variables. Landslide points were buffered to approximate scar area using the radius of a circle defined by the mean landslide scar area determined from previous shallow landslide mapping (Smith et al., 2021). Non-landslide points were selected randomly within each study area from locations outside the buffered areas surrounding landslide points. The selection of non-landslide point locations was repeated five times for each study area to provide a measure of variability associated with selection of point locations (Smith et al., 2021). For each selection, the number of non-landslide points was set to equal the number of mapped landslides (Heckmann et al., 2014; Goetz et al., 2015; Chen et al., 2017).

## 2.6. Logistic regression

Binary logistic regression (BLR) was used to relate landslide

presence/absence to the spatial explanatory variables. Explanatory variable data for all landslide and non-landslide locations were combined for analysis and continuous variables were standardised (centred around the mean and scaled by standard deviation). Standardisation allows the absolute size of estimated regression coefficient values to be interpreted as a measure of variable importance (Lombardo and Mai, 2018). We compare three sets of variables to assess how initially using only landscape variables and then sequentially adding intra-event (IE) and pre-event (PE) rainfall variables affect model outputs. The three variable sets comprise 1) topographic (i.e., slope, aspect, flow accumulation, curvature), land cover, and rock type (TLR); 2) TLR + IE; and 3) TLR + IE + PE inputs. The third set makes all variables available for potential inclusion in the model.

For each variable set, automated variable selection was performed using the Least Absolute Shrinkage and Selection Operator (LASSO) (Tibshirani, 1996; Lombardo and Mai, 2018). LASSO allows simultaneous variable selection and coefficient estimation to generate sparse models and reduce over-fitting. LASSO adds a penalty term to the log-likelihood function of the logistic regression that determines the number of variables where coefficient values are shrunk to zero by minimising model error (Hastie et al., 2009; Lombardo and Mai, 2018). An optimal penalty term was selected using cross-validation to be within one standard error above the minimum error (Zweifel et al., 2021). We employ group LASSO to handle categorical variables (e.g., rock type, land cover) (cf. Zweifel et al., 2021). In group LASSO, the coefficients of all classes within a given categorical variable are either selected (i.e., all non-zero) or excluded (i.e., all zero) as a group.

BLR was implemented using group LASSO within a  $k$ -fold cross-validation procedure applied to the three variable sets. The datasets were randomly shuffled and split into  $k = 5$  folds where  $k - 1$  folds were used for model fitting and each remaining fold used once for testing. For each data split, the value of the LASSO penalty term was first determined by 5-fold cross-validation using only data selected by the  $k - 1$  folds. This penalty value was then used in model fitting and testing. The procedure was repeated to produce a total of 100 data partitions and the median of fitted (non-zero) regression coefficients as well as their rate of inclusion in the model were recorded. Rainfall variables were limited to a positive association with landslide occurrence during cross-validation. This constraint is physically based given higher antecedent moisture and event rainfall increase porewater pressure and the likelihood of slope failure (Crozier, 1999; Guzzetti et al., 2007; Bordoni et al., 2015).

We test sensitivity to sample size by repeated random sampling of the landslide presence/absence dataset in equal proportions then running the BLR model for sample sizes of  $n = 400, 800, 1600, 3200, 6400, 12,800$  as well as all data. The purpose of this comparison was to assess how increasing sample size affects model predictive performance, coefficient values, and the frequency of variable inclusion. Smaller samples tend to produce more varied and less accurate predictions whereas larger samples may experience issues with spatial autocorrelation that violates the logistic regression assumption of independent observations or risks model overfitting (Heckmann et al., 2014). Spatial autocorrelation may inflate the effect size of variables (Mets et al., 2017). Generally decreasing sample size increases the average distance between observations and thus reduces spatial autocorrelation. Therefore, we assess how model performance, variable selection and coefficient values vary with sample size to inform selection of an optimum sample size for further analysis (Heckmann et al., 2014; Spiekermann et al., 2022).

We also test model sensitivity to the inclusion and exclusion of a single variable to assess its importance in univariate and multivariate contexts, respectively (Lombardo and Mai, 2018; Williams et al., 2022). This analysis compares univariate predictive power with the effect of excluding a single variable from a multivariate model, where the reduction in predictive performance is indicative of the variable's importance. We focus on testing the inclusion and exclusion of those variables that exhibited a 100 % inclusion rate in the BLR model with TLR + IE + PE inputs.

We used the gglasso v1.5 package in R to implement the group LASSO (Yang and Zou, 2015). Model classification performance was evaluated using receiver operating characteristic (ROC) curves and calculation of the area under curve (AUC) using the ROCR v1.0-11 package (Sing et al., 2005). ROC curves plot the true positive rate (sensitivity) versus the false positive rate ( $1 - \text{specificity}$ ) across all potential probability cut-off values (0–1). An AUC value of 0.5 indicates classification no better than a random guess whereas an AUC of 1 corresponds to perfect classification.

## 2.7. Landslide spatial density

The BLR analysis provided information on those spatial variables influencing susceptibility to shallow landslide occurrence. However, it does not provide insight into the magnitude of landslide response to storm events and how this varies in relation to those variables found to influence susceptibility. To address the magnitude of landslide response, we use the landslide point data to compute the spatial density of landslides and relate these data to spatial patterns in slope, land cover, rock type, and rainfall. Each study area was divided into a  $250 \times 250$  m ( $62,500 \text{ m}^2$ ) grid. This produced a total of 16,831 grid squares across the four study areas. The number of landslide points was counted per grid square to give the landslide density. The choice of grid size was determined with reference to the explanatory variable data to ensure sufficient grid squares were available once the data was partitioned to represent the main land covers and rock types present within the

dataset.

Variable information was summarised per grid square. For continuous variables such as slope and rainfall, the mean value was determined per grid, and these values were then grouped into bins for analysis. The spatial intersection of categorical variables was calculated to determine the proportional extent of individual classes per grid. These data were used to partition grids into those containing only pasture or forest cover. Pasture comprises areas mapped as 'low producing grassland' and 'high producing grassland' while forest contains areas classified as 'indigenous forest', 'broadleaf indigenous hardwoods', and 'exotic forest' in the NZ LCDB. The pasture and forest grids were further partitioned by rock type class, which was re-grouped into a) soft

**Table 2**  
Mean landslide densities and the number of grid squares per land cover and rock type.

Land cover	Rock type - grouped	Rock type – individual classes	Grid n	Landslide n	Mean landslide density (scars per km <sup>2</sup> )
Pasture	All	All	2441	7197	47
	Soft sedimentary rocks	Sandstone or coarse siltstone – massive; Mudstone or fine siltstone – massive; Mudstone or fine siltstone – jointed; Mudstone or fine siltstone – banded	762	4649	98
	Hard sedimentary rocks	Greywacke; Greywacke – weathered; Argillite	103	131	20
	Ashes older than Taupo pumice	Ashes older than Taupo pumice	1549	2402	25
	Volcanic rocks	'Soft' volcanic rocks - weathered; Lava, ignimbrite and other 'hard' volcanic rocks	27	15	8.9
	All	All	1898	614	5.2
	Soft sedimentary rocks	Sandstone or coarse siltstone – massive; Mudstone or fine siltstone – massive; Mudstone or fine siltstone – jointed; Mudstone or fine siltstone – banded	317	131	6.6
	Hard sedimentary rocks	Greywacke; Greywacke – weathered; Argillite	804	376	7.5
	Ashes older than Taupo pumice	Ashes older than Taupo pumice	348	39	1.8
	Volcanic rocks	'Soft' volcanic rocks - weathered; Lava, ignimbrite and other 'hard' volcanic rocks	429	68	2.5

sedimentary rocks, b) hard sedimentary rocks, c) ashes older than Taupo pumice, and d) volcanic rocks based on the NZ LRI (Table 2). Grid classification by rock type was based on a grid square containing only a single rock type class.

### 3. Results

#### 3.1. Model performance and sample size

Predictive performance of the BLR model varied with inputs and sample size. The TLR variable set consistently produced lower median AUC values (range = 0.708–0.809) compared to the TLR + IE (0.757–0.838) and TLR + IE + PE (0.759–0.842) inputs irrespective of sample size (Fig. 5). The inclusion of intra-event rainfall variables resulted in a larger increase in median AUC compared to TLR, while a minor increase in AUC was achieved with the further addition of pre-event rainfall. For a sample size of  $n = 6400$  or above, the increase in median AUC plateaued ( $>0.795$ ) and the inter-quartile range (IQR) decreased from a range of 0.064–0.095 to  $<0.020$ .

The rate of variable inclusion generally increased with sample size based on analysis of the TLR + IE + PE input (Fig. 6a). Consistent variable inclusion across sample sizes provides a measure of variable importance. Only slope was selected in all model iterations across all sample sizes. Normalised total event rainfall ('event rainfall norm' in Fig. 6a) and normalised 10-day pre-event rainfall accumulation ('10d accum norm') were selected in all iterations except for the smallest sample size. Other variables with high inclusion rates across most sample sizes include normalised maximum 12-hour rainfall intensity ('i12h norm') and those related to land cover.

The variation in coefficient values with sample size is shown in Fig. 6b-g for those variables with the highest inclusion rates and the largest absolute coefficient values. For sample sizes of  $n = 3200$  and above, coefficient values are generally consistent, except for indigenous forest (Fig. 6g) and to a lesser extent pasture (Fig. 6e) which increase in absolute terms. This suggests some inflation of effect size related to spatial autocorrelation. For smaller sample sizes, coefficients tend to be closer to zero. This may reflect issues related to smaller samples where

input variables may be inadequately represented, model uncertainty is larger, and coefficients more likely to be insignificant (Heckmann et al., 2014). Variable selection rates were consistent between  $n = 12,800$  and all data (Fig. 6a), while model predictive performance was similar (Fig. 5). Taken together, these findings support a focus on the  $n = 12,800$  sample size to maximise model predictive performance and representation of variables while constraining the potential influence of spatial autocorrelation. The  $n = 12,800$  sample represents 25 % of the complete presence/absence dataset.

#### 3.2. Factors influencing landslide susceptibility

Variable inclusion rates were reasonably consistent between TLR, TLR + IE, and TLR + IE + PE sets based on a sample size of  $n = 12,800$  (Fig. 7). Comparing across grouped variables, land cover followed by slope and rainfall had the largest influence based on the absolute size of coefficients. Rock type, aspect and curvature had less influence on the model while flow accumulation had negligible effect. In terms of specific classes, pasture, slope, and harvested forest had the largest positive coefficient values (increasing landslide susceptibility). In contrast, indigenous and exotic forest had the largest absolute coefficient values with a negative effect (decreased susceptibility).

The absolute size of coefficient values for different rock types generally decreased with the inclusion of IE and PE variables. Nonetheless the direction of influence mostly remained the same. Only the 'Greywacke – weathered', 'Greywacke', and 'Hard volcanic rocks (incl. lavas, ignimbrite)' classes switched from positive to negative coefficient values with the inclusion of rainfall data (Fig. 7). The change in coefficient values reflects the inclusion of a rainfall effect in the model that was otherwise expressed via the rock type coefficients in the absence of spatial rainfall information.

The intra-event rainfall variables 'i12h norm' and 'event rainfall norm' exhibited positive coefficients and were included in all model iterations for the TLR + IE and TLR + IE + PE variable sets (Fig. 7). The addition of PE variables led to the selection of '10d accum norm' for all repetitions (Fig. 7b) and resulted in the inclusion of shorter duration intensities ('i60min norm', 'i2h norm') in some repetitions. It seems

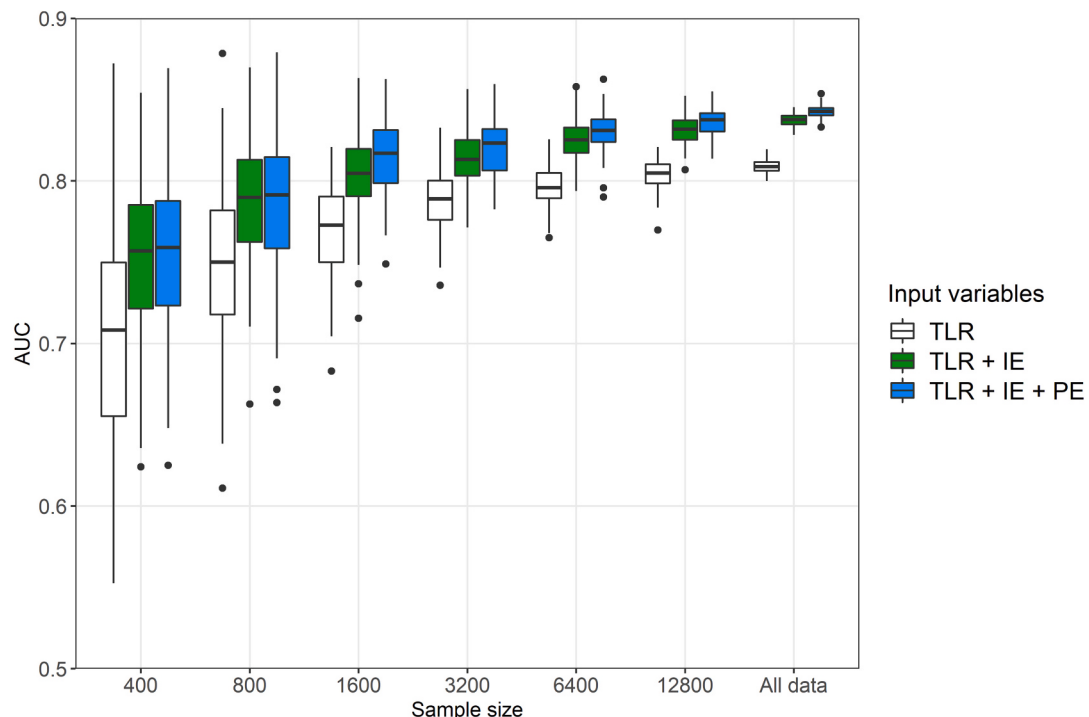


**Fig. 5.** Boxplots showing the variation in AUC values from 100 model iterations for different sample sizes and input variable sets.

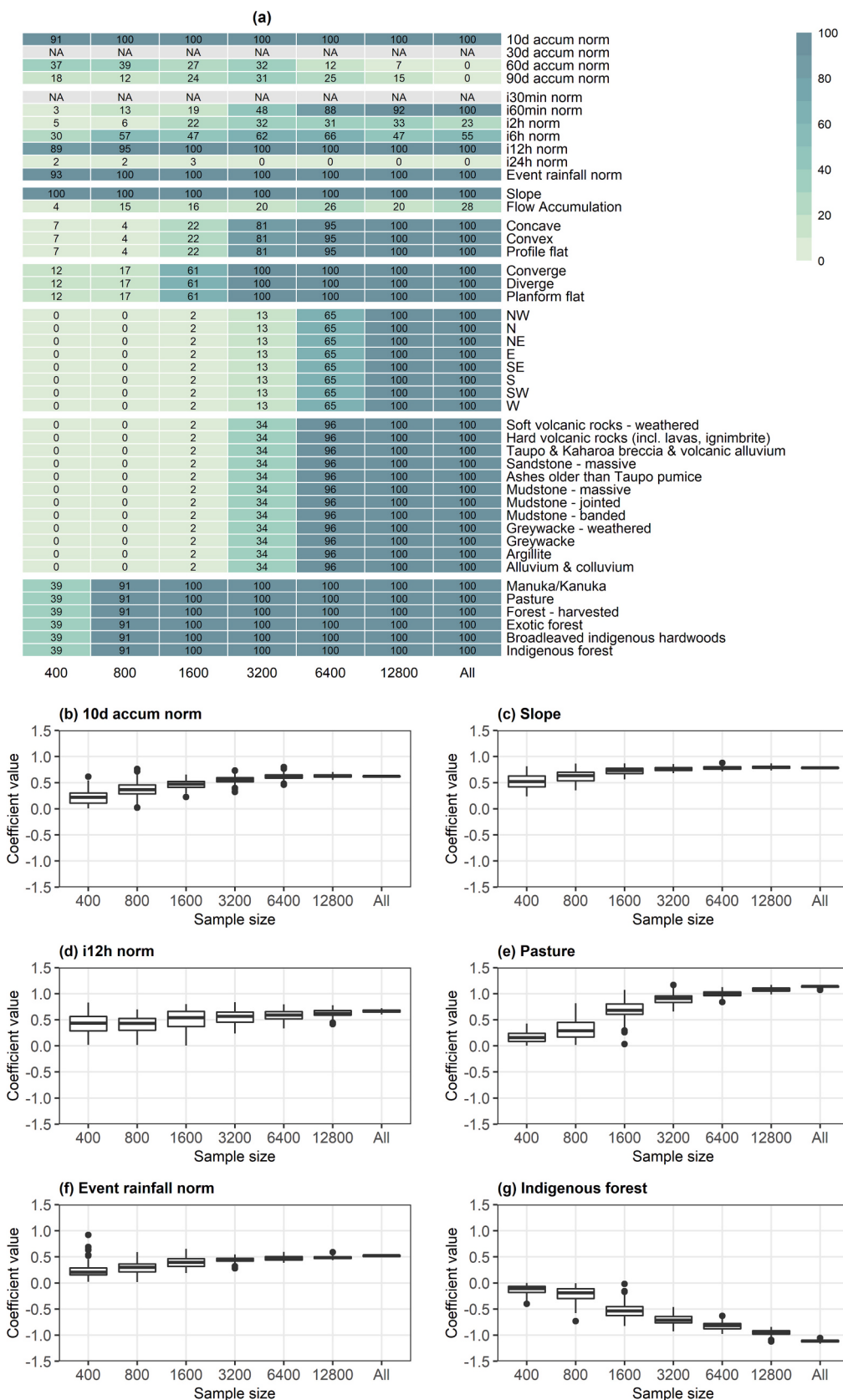


**Fig. 6.** Sample size effect on a) variable selection rate and b) to g) fitted coefficient values for selected variables based on 100 model iterations for the TLR + IE + PE variable set. The rainfall variables 'i30min norm' and '30d accum norm' (labelled NA) were excluded as they did not exhibit a positive association with landslide occurrence.

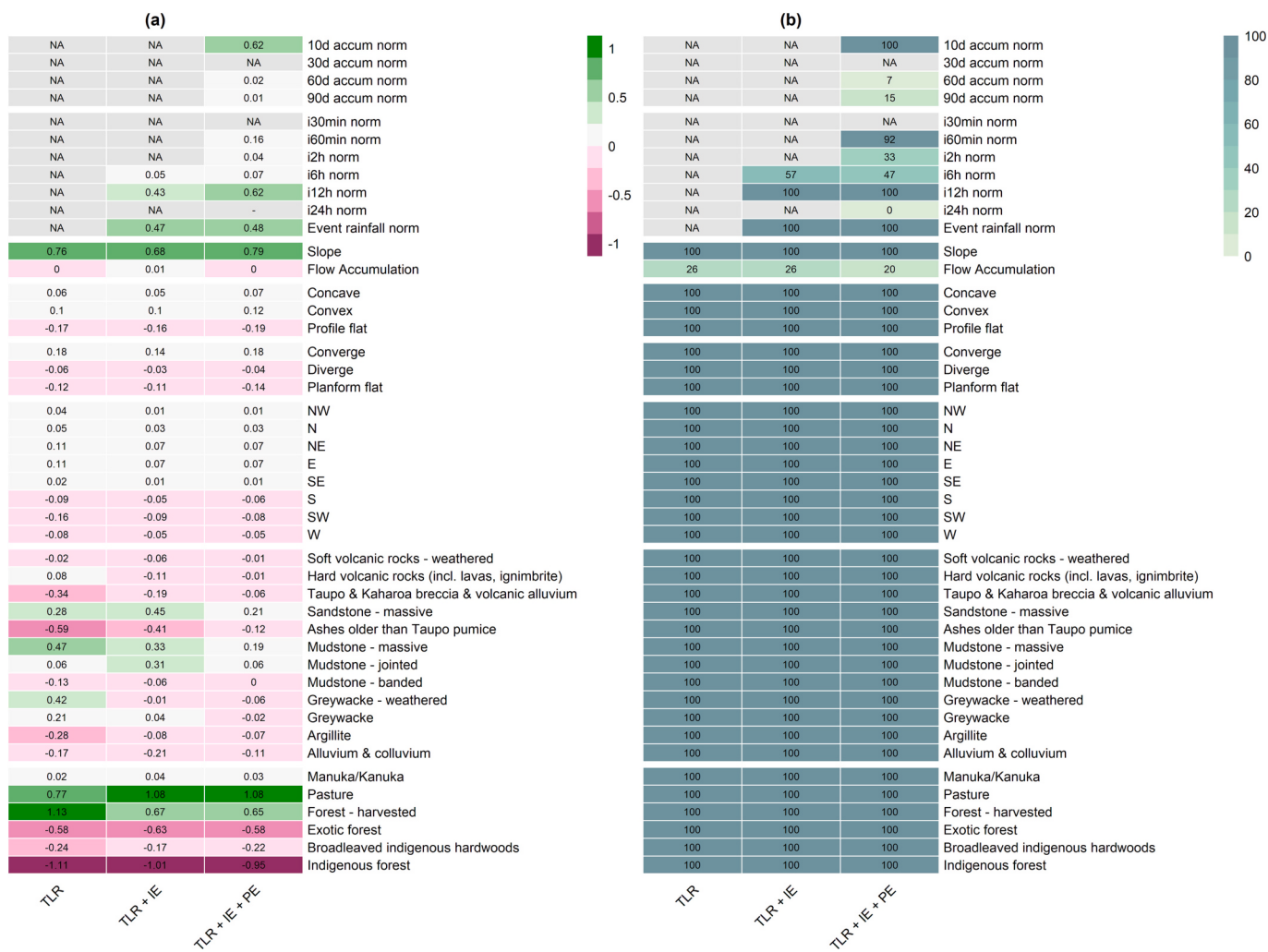


**Fig. 7.** Heat maps showing a) median of non-zero coefficient values and b) variable selection rate from 100 model iterations for the three sets of input variables based on a sample size of  $n = 12,800$ .

recent prior rainfall may increase the association between landslide occurrence and shorter-duration intense rainfall (60 min – 12 h) within longer-duration events. In contrast, the coefficient for ‘event rainfall norm’ was barely affected by the inclusion of pre-event rainfall data.

The effects of single variable inclusion versus exclusion on model performance are shown in Fig. 8. The variables with the highest median AUCs in a univariate model were slope, ‘event rainfall norm’, ‘i12h norm’, and rock type (Fig. 8a). The removal of a single variable from the multivariate model resulted in the largest reductions in median AUC for land cover, slope, ‘i12h norm’, and rock type, indicating the importance of these variables in a multivariate context (Fig. 8b). Besides slope, other topographic variables (i.e., aspect, profile curvature, planform curvature) had less influence on performance of either univariate or multivariate models. ‘10d accum norm’ was not selected for inclusion in the univariate model (hence the model produced an AUC = 0.5). This contrasts with the apparent importance of this variable based on the frequency of selection when testing the TLR + IE + PE model with different sample sizes (Fig. 6a). Pre-event rainfall on its own provides no discrimination of landslide presence/absence whereas when combined with other variables it improves prediction.

### *3.3. Factors influencing landslide spatial density*

Landslide densities are summarised in Table 2 by land cover and rock type. The selection of grid squares with complete coverage of pasture or

forest for selected rock types equated to  $n = 4339$  of 16,831 across the four study areas. Mean landslide densities under pasture and forest were 47 versus 5.2 scars  $\text{km}^{-2}$  irrespective of rock type or rainfall patterns. Fewer landslides were observed in forest, reflecting the lower susceptibility to land instability and possibly some missing data associated with forest cover obscuring features. However, use of high-resolution imagery (0.5 m) and the comparison of before/after imagery should limit under detection of landslides in forested areas.

The mean landslide density for pasture masks considerable variation related to rock type, which ranges from 8.9 scars km<sup>-2</sup> for volcanic rocks to 98 scars km<sup>-2</sup> for soft sedimentary rocks (Table 2). The range in landslide densities between different rock types under forest is much lower, spanning 1.8 to 7.5 scars km<sup>-2</sup>, which suggests landslide occurrence is relatively insensitive to rock type under forest versus pasture areas. Comparing pasture to forest areas irrespective of rock type or rainfall shows a 9.1-fold increase in landslide density (Table 3). This pasture-to-forest ratio increases to a 15-fold difference for soft sedimentary rocks. In contrast, hard sedimentary and volcanic rocks display pasture-to-forest ratios of 2.7 and 3.5, respectively (Table 3).

Storm rainfall influences spatial patterns in landslide density. The BLR model with LASSO identified '112h norm' and 'event rainfall norm' as the most important intra-event rainfall variables. Moreover, rainfall exhibited some co-variation with land cover and rock type (e.g., higher rainfall tended to occur over forested ranges). To reduce the potential influence of rainfall patterns and better identify differences that may be

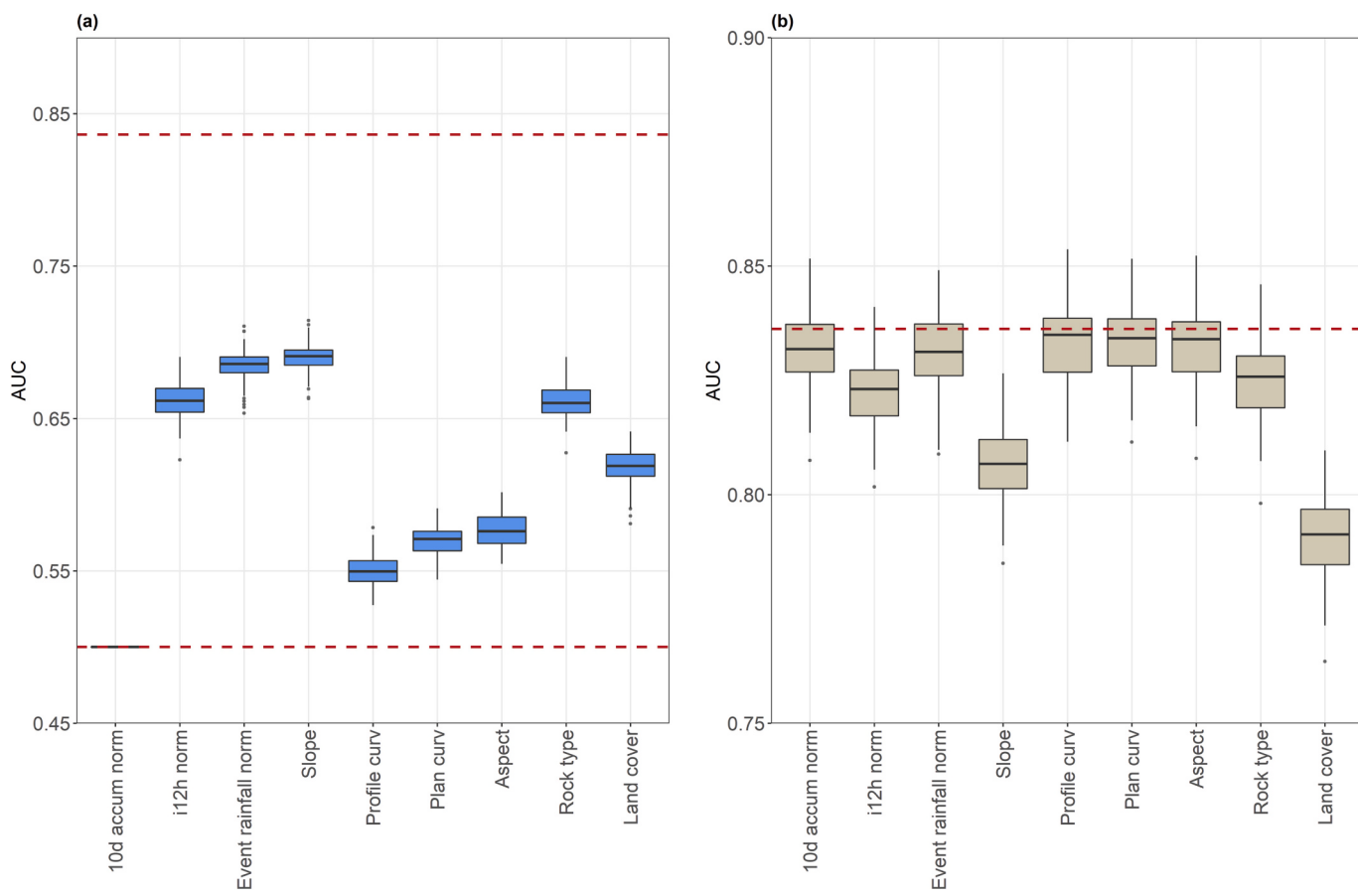


**Fig. 8.** Boxplots of AUC values for 100 model repetitions resulting from a) inclusion of a single variable (where upper dashed line is the median AUC for the full model and lower dashed line is random) and b) exclusion of a single variable (where dashed line is the median AUC for the full model) for those variables with a 100 % inclusion rate based on a sample size of  $n = 12,800$  for TLR + IE + PE inputs.

**Table 3**

Comparison of shallow landslide densities with and without rainfall normalisation between pasture and forest areas by rock type and slope class.

	Comparison	Pasture-to-forest landslide density ratio		
		Non-normalised ( $p$ -value)	i12h normalised ( $p$ -value)	Event rainfall normalised ( $p$ -value)
Rock type	All	9.1*	11*	13*
	Soft sedimentary rocks	15*	19*	15*
	Hard sedimentary rocks	2.7 (0.103)	2.8 (0.083)	2.3 (0.104)
	Ashes older than Taupo pumice	14*	12*	24*
	Volcanic rocks	3.5*	9.8*	7.0*
	s < 15	5.1*	6.8*	16*
Slope (°)	15 ≤ s < 20	17*	24*	30*
	20 ≤ s < 25	13*	18*	22*
	25 ≤ s < 30	12*	13*	16*
	30 ≤ s < 35	25*	26*	32*
	s ≥ 35	49*	50*	55*

\* p-value < 0.001.

attributable to rock type or slope, we normalised landslide density using the two rainfall variables. Mean grid values of 'i12h norm' (range = 0.30–1.68) and 'event rainfall norm' (0.05–0.38) were multiplied by 10 and 100, respectively, to produce rainfall indices with values >1 and

these were used to normalise densities.

Normalisation mostly increased pasture-to-forest landslide density ratios (Table 3). This result reflects typically higher rainfall over forested areas that correspond with lower landslide densities compared to pasture. In other words, significantly less rainfall is required to produce an equivalent landslide density for pasture compared to forest. Despite the difference in ratios, the statistical results were consistent irrespective of our treatment of the landslide density data (Table 3).

Landslide densities were more sensitive to slope in pasture compared to forested areas. Mean densities normalised by 'i12h norm' and 'event rainfall norm' increased with slope class under pasture (Fig. 9). The largest relative increases in normalised density for pasture areas occurred between slopes <15° versus 15–20°, while there was a consistent increase in densities for slopes over 30°. In contrast, normalised landslide densities displayed little variation with slope class in forested areas. Pasture-to-forest density ratios showed that the largest differences between land covers occurred for slopes over 30°, and differences were statistically significant ( $p < 0.001$ ) for all slope classes (Table 3).

Soft sedimentary rocks produced the largest number of landslides with the highest areal densities across the study areas. We focus on this rock type to assess how landslide density (non-normalised) varied in response to intra-event rainfall as represented by 'i12h norm' and 'event rainfall norm', irrespective of variations in slope. Mean values of 'i12h norm' and 'event rainfall norm' per grid square were grouped into four classes, which ensured sufficient data per class (Fig. 10).

For pasture areas with 'i12h norm' values <1.25, mean landslide densities ranged 50–72 scars km<sup>-2</sup> versus >1.25 (i.e., 12 h intensity 25 % above the 10-year recurrence interval intensity) with 234 scars km<sup>-2</sup>.

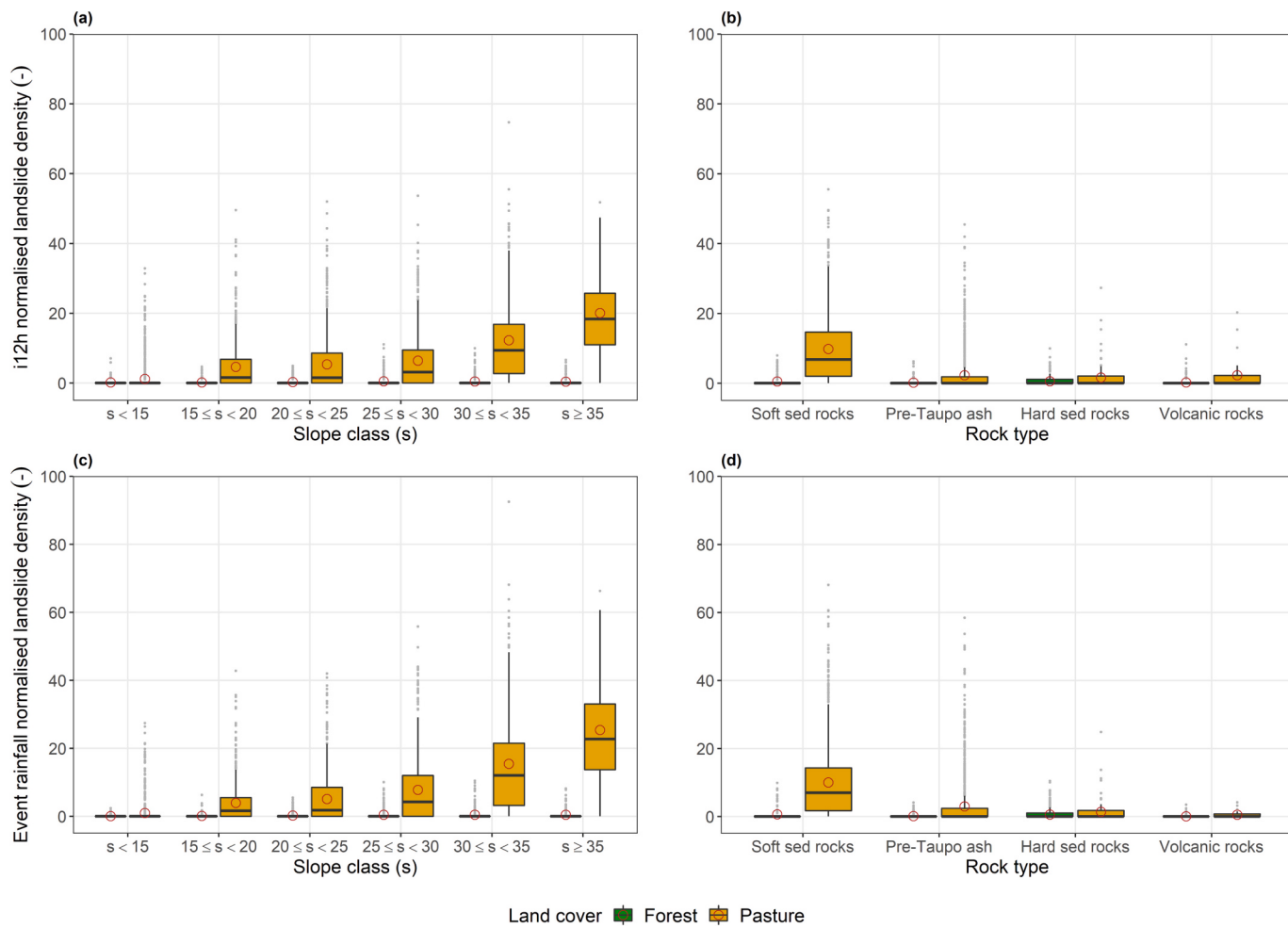


**Fig. 9.** Boxplots showing variation in landslide densities for pasture and forest cover normalised by 'i12h norm' and 'event rainfall norm' for slope class (degrees) and rock type. The number of grid squares per boxplot range between 69–1816 and 27–1549 for slope and rock type, respectively.

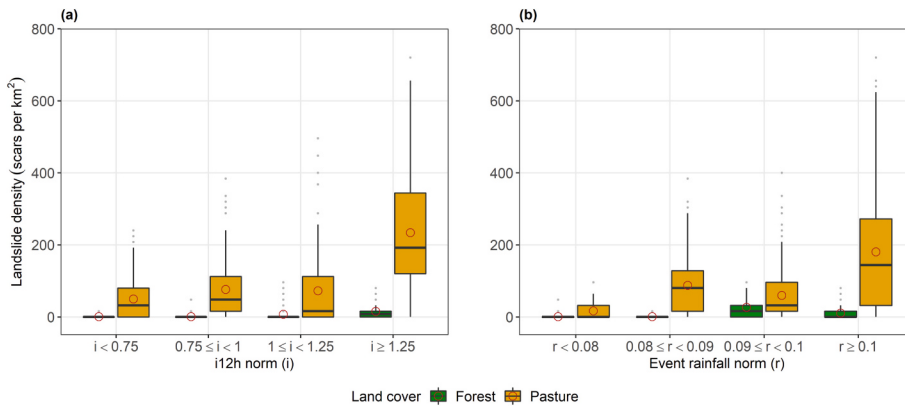


**Fig. 10.** Boxplots showing variation in shallow landslide densities with a) 'i12h norm' and b) 'event rainfall norm' for pasture and forest cover on soft sedimentary rocks. Red circles represent mean values. The number of grid squares per boxplot range between 45–299 and 23–345 for 'i12h norm' and 'event rainfall norm', respectively. (For interpretation of the references to colour in this figure legend, the reader is referred to the web version of this article.)

A similar pattern was evident for 'event rainfall norm' where values  $<0.1$  ranged 17–87 scars  $\text{km}^{-2}$  versus  $>0.1$  (i.e., storm rainfall exceeding 10 % of mean annual rainfall) with 181 scars  $\text{km}^{-2}$ . In contrast, forested areas exhibited a much lower range in mean landslide densities across the four classes (Fig. 10), spanning 0.7–15 and 0.5–27 scars  $\text{km}^{-2}$  for 'i12h norm' and 'event rainfall norm', respectively. The difference in landslide densities between pasture and forest was

statistically significant in all cases ( $p < 0.005$ ).

#### 4. Discussion

Geo-environmental factors had the largest influence on susceptibility to shallow landslides based on the regression coefficients in the present study. Pasture (median coefficient = 1.08) and indigenous forest

(−0.95) exerted the most influence on susceptibility when all variables (i.e., TLR + IE + PE) were available for potential inclusion in the model. Other land covers such as harvested forest (0.65) and exotic forest (−0.58) contributed to increased and reduced susceptibility, respectively. Slope (0.79) was the third most important input while other topographic (i.e., aspect, curvature, flow accumulation) and rock type variables had less influence. The inclusion of rainfall variables, namely ‘i12h norm’ (0.62), ‘10 d accum norm’ (0.62), and ‘event rainfall norm’ (0.48), improved prediction compared to geo-environmental factors only. The three variable sets, TLR, TLR + IE and TLR + IE + PE, produced median AUCs of 0.805, 0.832, and 0.838, respectively, based on the sample size ( $n = 12,800$ ) selected to maximise performance while limiting spatial autocorrelation.

The importance of land cover for landslide susceptibility reflects the role of trees in stabilising slopes. Trees provide root reinforcement and may reduce soil moisture and thus pore water pressures through increased canopy interception and evapotranspiration (Stokes et al., 2014; Phillips et al., 2021). These effects underpin the opposing influence on susceptibility of pasture versus long-established indigenous forest, while the relative influence of the smaller pioneer scrub species mānuka and kānuka is situated between these land cover end members. Forest harvesting increases susceptibility compared to pre-harvest exotic forests but harvested areas retain residual reinforcement that diminishes as roots decay (Phillips et al., 2018). This may explain why harvested forest has a lower positive influence on susceptibility compared to pasture.

The lesser influence of rock type on susceptibility in the present study may relate to the shallow depth of landslides that occur in regolith. Rock type indirectly influences susceptibility as it is effectively a proxy for potential differences in regolith properties (e.g., shear strength, hydraulic conductivity) that may directly affect susceptibility but lack spatial representation (Crozier et al., 1980; Smith et al., 2021). Differences in these properties for the same mapped rock type within and between study areas, in addition to potential mapping errors, may reduce the apparent influence of rock type on susceptibility (Smith et al., 2021). Nonetheless, the direction of influence based on the TLR + IE + PE variable set (Fig. 7) is generally consistent with previous assessments where the presence of soft sedimentary rocks (Table 2) increase susceptibility while hard sedimentary rocks, volcanic rocks, and tephra covers tend to reduce susceptibility (Basher et al., 2016).

The contribution of planform curvature included the contrasting influence of convergent (0.18) versus divergent (−0.04) zones on susceptibility (Fig. 7). This result is consistent with observations that convergent areas such as hillslope hollows or zero-order basins tend to concentrate flow, thereby increasing soil saturation and the potential for slope failure (Giuseppe et al., 2016; Crozier, 2017). Convex and concave zones defined by their profile curvature varied with slope position and both had a minor positive association with susceptibility. Northern and eastern aspects correspond with a small increase in susceptibility, which aligns with previous findings for shallow landslides in New Zealand's hill country (Gao and Maro, 2010; Spiekermann et al., 2022).

The influence of rock type on susceptibility decreased with the inclusion of spatial rainfall information. The range in coefficient values for the different rock types were −0.59–0.47 and −0.12–0.21 for TLR versus TLR + IE + PE, respectively. The results show how accounting for spatial patterns in event rainfall may reduce or reverse the influence of categorical variables such as rock type. For example, the inclusion of rainfall produced a switch from positive to negative coefficient values for ‘Greywacke – weathered’, ‘Greywacke’, and ‘Hard volcanic rocks (incl. lavas, ignimbrite)’. These rock types are generally associated with lower landslide susceptibility compared to soft sedimentary rocks (Basher et al., 2016). The switch occurred because higher normalised rainfall tended to co-vary with these rock types in the Hunua Ranges and Coromandel study areas where they mostly occur. Such co-variation may arise because the ranges comprising more resistant lithologies tend to correspond with higher event rainfall associated with orographic

effects. In the absence of rainfall information, these rock type classes expressed the positive influence of higher rainfall, in contrast to their expected influence on susceptibility.

Short-term (10 d) pre-event rainfall exhibited a similar level of influence on susceptibility as intra-event rainfall. In contrast, longer duration pre-event rainfall accumulations (60–90 d) had negligible effect. On a univariate basis, ‘10 d accum norm’ was unable to improve on random classification (Fig. 8a), whereas when included alongside other variables it produced a small improvement in prediction and increased the influence of shorter-duration intra-event intensities (60 min–12 h). This result suggests recent prior rainfall may increase landslide triggering in response to shorter duration intense rainfall within longer duration events ( $\geq 48$  h). This finding is broadly consistent with Steger et al. (2023) who reported that higher levels of precipitation during a period 1–30 days prior to an event decreased the amount of precipitation required to trigger shallow landslides. However, the analysis by Steger et al. (2023) focused on daily precipitation, thus their findings do not extend to how antecedent conditions might affect the landslide response to shorter duration rainfall intensities.

Generally multi-temporal landslide inventories are considered preferred sources of landslide data for susceptibility modelling (Reichenbach et al., 2018). However, Smith et al. (2021) found comparable model performance for event versus multi-temporal landslide inventories, which was attributed to high event landslide densities. In the present study, AOIs were selected to span a wider range in rainfall, whereas in Smith et al. (2021) AOIs were targeted towards areas most impacted by landslides, which includes some overlap with the present study (namely Wairamarama and Whanganui – west). Despite not targeting AOIs to only the most impacted areas, model predictive performance in the present study was reasonable (i.e., AUC > 0.8) when using geo-environmental variables and excluding spatial rainfall information. This result supports the previous finding that event inventories may not necessarily compromise the predictive performance of landslide susceptibility models. However, the lack of spatial rainfall information in models using event data may reduce the reliability of statistical inferences based on model coefficients.

The AOIs cover a large range in storm rainfall. Estimated mean (range, duration) event rainfall totals were 115 (69–191, 48 h), 139 (128–146, 48 h), 205 (149–271, 48 h), and 441 (221–654, 120 h) mm for the Whanganui, Wairamarama, Hunua Ranges, and Coromandel study areas, respectively, based on the radar QPEs. The mean (range) value of the AOIs for the 24 h rainfall maxima amounted to 113 (69–181), 75 (67–80), 201 (143–255), 214 (95–346) mm, respectively. Previous estimates of rainfall thresholds for shallow landslides in New Zealand suggest events exceeding 120 mm in 24 h or 125–200 mm in 48 h were likely to trigger a landslide response (Glade, 1998; Reid and Page, 2002; Basher et al., 2020). Both the event total and 24 h rainfall maxima exceed the estimated thresholds in all cases except Wairamarama. Notably, those AOIs with the lowest 24 h rainfall maxima (Whanganui and Wairamarama) have the highest spatial landslide densities (34 and 43 scars  $\text{km}^{-2}$ ). These densities compare to 14 and 5.4 scars  $\text{km}^{-2}$  for the Hunua Ranges and Coromandel AOIs, respectively. The level of exceedance of typical rainfall thresholds is thus a poor indicator of the magnitude of landslide response.

Generic rainfall thresholds are problematic because they ignore variations in climate and landscape factors influencing susceptibility (Marc et al., 2019). The Whanganui and Wairamarama AOIs are characterised by predominantly pasture cover and soft sedimentary rocks or volcanic ash beds, whereas the Hunua Ranges and Coromandel AOIs contain greater forest cover and generally more resistant rock types. Pasture-to-forest ratios in landslide spatial density range 9.1–13 across rock types (Table 3), while higher ratios occurred on soft sedimentary rocks and volcanic ash beds (12–24). The difference in spatial density between pasture and forest for terrain on hard sedimentary rocks was insignificant. Thus, certain rock types may partly offset the effect of land cover on landslide susceptibility. However, forest cover reduced the

sensitivity of landslide density to variations in slope, rainfall, and rock type, in contrast to pasture (Figs. 9 and 10). These findings show how targeted, long-term afforestation may be used to reduce landslide densities irrespective of slope, rock type or rainfall, at least for the range of terrain and rainfall conditions in the present study.

Pasture covered slopes on soft sedimentary rocks represent the most susceptible terrain with the lowest rainfall thresholds for triggering shallow landslides. This terrain produced a significant 3.5-fold increase in the mean landslide spatial density ( $234 \text{ vs. } 66 \text{ scars km}^{-2}$ ,  $p < 0.005$ ) when the maximum 12 h intensity was  $\geq 25\%$  above the 10-y recurrence interval intensity compared to lower intensities and a 2.7-fold increase ( $181 \text{ vs. } 67 \text{ scars km}^{-2}$ ,  $p < 0.005$ ) when the event total was  $\geq 10\%$  of mean annual rainfall compared to lower rainfall (Fig. 10). In contrast, forested areas on soft sedimentary rocks produced much lower landslide densities ('i12h norm' = 15 vs.  $3.4 \text{ scars km}^{-2}$  and 'event rainfall norm' = 10 vs.  $4.8 \text{ scars km}^{-2}$ ), although the relative differences in landslide densities corresponding to rainfall above and below the thresholds were comparable to pasture.

The analysis of spatial patterns in storm rainfall in relation to the magnitude of landslide response provides quantitative evidence for Crozier's (2017) cell model for multiple-occurrence regional landslide events (MORLEs). The rainfall thresholds, particularly for the 'i12h norm', show a step-change in landslide spatial densities on pastoral land that may distinguish the so-called 'core' zone with maximum landslide impacts from the middle and peripheral zones (Fig. 4e). However, Crozier's (2017) suggestion that mitigations based on reducing the influence of susceptibility factors will be rendered ineffective within the 'core' zone is not supported by the data in the present study. The comparatively low landslide densities in forested areas show how targeted afforestation of susceptible pastoral land may provide effective mitigation, even under very high rainfall. We did not discriminate between forest type (e.g., exotic vs. native) or age in the present study as there was insufficient data to support further partitioning. As trees grow, they contribute to slope stability via increasing hydrological and root reinforcement effects (Phillips et al., 2021), thus increasing forest maturity should generally correspond with decreasing landslide densities in response to storm rainfall.

The sensitivity of landslide densities to rainfall intensity, particularly 'i12h norm' has important implications for landscape responses to climate change. Storm magnitude is projected to increase with warming across New Zealand leading to increased landslide erosion on susceptible terrain (Neverman et al., 2023). The average percentage increase in rainfall depth across New Zealand per  $1^\circ$  increase in temperature ranges 8.5–10.1 % (2–100 y ARI) for 12-h duration, while the 10 y ARI event corresponds to a 9.5 % increase in rainfall depth (Ministry for the Environment, 2018). By 2081–2100, the projected mean increase in temperature across New Zealand ranges 0.59–2.58 degrees (Ministry for the Environment, 2018). Thus, the average percentage increase in rainfall depth for the 12-h duration (10 y ARI) at the highest projected level of warming amounts to 25 %. Our results show that this level of increase in rainfall over 12 h may produce a disproportionately large increase in landslide spatial density, although reduced antecedent soil moisture with warming could partly offset rainfall intensity-related increases in landslide density (Maraun et al., 2022).

An increase in landslide density poses a significant challenge for managing the impacts of climate change in pastoral hill country on weak sedimentary rocks, terrain which is widespread across the North Island of New Zealand. Landslide-triggering storm events reduce agricultural production, increase sedimentation, reduce freshwater quality, deliver forestry debris to streams, and threaten infrastructure as well as sites of cultural significance to Māori (Dominati et al., 2014; Phillips et al., 2018, 2021; Smith et al., 2021; Neverman et al., 2023). Substantial additional investment in erosion control may be required to mitigate potential impacts from landslide erosion at least partially under climate change.

## 5. Conclusions

We found land cover and slope exerted the largest influence on shallow landslide susceptibility ahead of intra-event rainfall intensities and pre-event rainfall accumulations for study areas spanning a range of terrain and rainfall conditions. Rock type had a lesser influence on susceptibility. Higher rainfall tended to co-vary with elevated ranges comprising more resistant lithologies, thus the influence of rock type decreased with the inclusion of spatial rainfall information that improved model prediction. Of the rainfall variables, maximum 12 h rainfall normalised by the 10-y recurrence interval intensity and the 10-d pre-event accumulation normalised by mean annual rainfall had the most influence on susceptibility. Longer pre-event accumulation periods had negligible effect. On a univariate basis, 10 d pre-event rainfall was unable to improve on random classification but when combined with other variables it increased the influence of shorter-duration maximum intensities (60 min – 12 h).

The extent to which storm rainfall exceeded typical thresholds for triggering landslides in New Zealand was a poor indicator of the landslide response magnitude. In the present study, the most susceptible terrain comprises pasture on weak sedimentary rocks, while forested areas and terrain on hard sedimentary or volcanic rocks or with tephra covers exhibited lower landslide spatial densities. Forest cover reduced the sensitivity of landslide density to variations in slope, rainfall, and rock type, in contrast to pasture. We observed a 3.5-fold increase in mean landslide density once the maximum 12-h intensity was  $\geq 25\%$  above the 10-y recurrence interval intensity for pastoral land on weak sedimentary rocks. This threshold is consistent with the increase in 12-h rainfall by late century under the highest levels of projected warming in New Zealand, which suggests that the landslide response to storm rainfall could be significantly amplified by climate change. Our findings support targeted, long-term afforestation of the most susceptible pastoral land to achieve large reductions in landslide densities, even under very high rainfall.

## Declaration of competing interest

The authors declare that they have no known competing financial interests or personal relationships that could have appeared to influence the work reported in this paper.

## Data availability

Data will be made available on request.

## Acknowledgements

This research was supported by the New Zealand Ministry of Business, Innovation and Employment research program "Smarter Targeting of Erosion Control (STEC)" (Contract C09X1804) and the Strategic Science Investment Fund (SSIF) allocated to Landcare Research. We thank Michael Crozier and an anonymous reviewer for providing helpful comments that improved the manuscript.

## References

- Basher, L.R., 2013. Erosion processes and their control in New Zealand. In: Dymond, J.R. (Ed.), *Ecosystem Services in New Zealand—Conditions and Trends*. Manaaki Whenua Press, Lincoln, New Zealand, pp. 363–374.
- Basher, L., Barringer, J., Lynn, I., 2016. Update of the Erosion Susceptibility Classification (ESC) for the proposed NES for Plantation Forestry - subdividing the High and Very High ESC classes. Ministry for Primary Industries Technical Paper No. 2016/12.
- Basher, L., Spiekermann, R., Dymond, J., Herzig, A., Hayman, E., Ausseil, A.-G., 2020. Modelling the effect of land management interventions and climate change on sediment loads in the Manawatu-Whanganui region. N. Z. J. Mar. Freshw. Res. 54, 490–511.

- Berenguer, M., Sempere-Torres, D., Hürlimann, M., 2015. Debris-flow forecasting at regional scale by combining susceptibility mapping and radar rainfall. *Nat. Hazards Earth Syst. Sci.* 15, 587–602.
- Betts, H., Basher, L., Dymond, J., Herzig, A., Marden, M., Phillips, C., 2017. Development of a landslide component for a sediment budget model. *Environ. Model. Softw.* 92, 28–30.
- Bordoni, M., Meisina, C., Valentino, R., Lu, N., Bittelli, M., Cherisch, S., 2015. Hydrological factors affecting rainfall-induced shallow landslides: from the field monitoring to a simplified slope stability analysis. *Eng. Geol.* 193, 19–37.
- Bowman, E.T., 2022. Chapter 12 Small landslides – frequent, costly and manageable. In: Davies, T., Rosser, N., Shroder, J.F. (Eds.), *Landslide Hazards, Risks, and Disasters*, 2nd ed. Elsevier, pp. 439–477.
- Burnett, N., Meyer, G.A., McFadden, L.D., 2008. Aspect-related microclimatic influences on slope forms and processes, northeastern Arizona. *J. Geophys. Res.* 113, F03002.
- Carey-Smith, T., Henderson, R., Singh, S., 2018. High Intensity Rainfall Design System – Version 4. NIWA Client Report No. 2018022CH Prepared for Envirolink.
- Catani, F., Lagomarsino, D., Segoni, S., Tofani, V., 2013. Landslide susceptibility estimation by random forests technique: sensitivity and scaling issues. *Nat. Hazards Earth Syst. Sci.* 13, 2815–2831.
- Cecinati, F., De Nict, A.C., Sawicka, K., Rico-Ramirez, M.A., 2017. Optimal temporal resolution of rainfall for urban applications and uncertainty propagation. *Water* 9, 762.
- Chen, W., Pourghasemi, H.R., Kornejady, A., Zhang, N., 2017. Landslide spatial modeling: introducing new ensembles of ANN, MaxEnt, and SVM machine learning techniques. *Geoderma* 305, 314–327.
- Chiang, S.-H., Chang, K.-T., 2009. Application of radar data to modeling rainfall-induced landslides. *Geomorphology* 103, 299–309.
- Crozier, M.J., 1996. Runout behaviour of shallow, rapid earthflows. *Z. für Geomorphol. Suppl.-Bd* 105, 35–48.
- Crozier, M.J., 1999. Prediction of rainfall-triggered landslides: a test of the antecedent water status model. *Earth Surf. Process. Landf.* 24, 825–833.
- Crozier, M.J., 2017. A proposed cell model for multiple-occurrence regional landslide events: implications for landslide susceptibility mapping. *Geomorphology* 295, 480–488.
- Crozier, M.J., Eyles, R.J., Marx, S.L., McConchie, J.A., Owen, R.C., 1980. Distribution of landslips in the Wairarapa hill country. *N. Z. J. Geol. Geophys.* 23, 5–6.
- Dominati, E.J., Mackay, A., Lynch, B., Heath, N., Millner, I., 2014. An ecosystem services approach to the quantification of shallow mass movement erosion and the value of soil conservation practices. *Ecosyst. Serv.* 9, 204–215.
- Emberson, R., Kirschbaum, D.B., Amatya, P., Tanyas, H., Marc, O., 2022. Insights from the topographic characteristics of a large global catalog of rainfall-induced landslide event inventories. *Nat. Hazards Earth Syst. Sci.* 22, 1129–1149.
- Entin, J.K., Robock, A., Vinnikov, K.Y., Hollinger, S.E., Liu, S., Namkhai, A., 2000. Temporal and spatial scales of observed soil moisture variations in the extratropics. *J. Geophys. Res.* 105, 865–877.
- Gao, J., Maro, J., 2010. Topographic controls on evolution of shallow landslides in pastoral Wairarapa, New Zealand, 1979–2003. *Geomorphology* 114, 373–381.
- Giuseppe, F., Simoni, S., Godt, J.W., Lu, N., Rigan, R., 2016. Geomorphological control on variably saturated hillslope hydrology and slope instability. *Water Resour. Res.* 52, 4590–4607.
- Glade, T., 1998. Establishing the frequency and magnitude of landslide-triggering rainstorm events in New Zealand. *Environ. Geol.* 35, 160–174.
- Goetz, J.N., Brenning, A., Petschko, H., Leopold, P., 2015. Evaluating machine learning and statistical prediction techniques for landslide susceptibility modelling. *Comput. Geosci.* 81, 1–11.
- Guzzetti, F., Peruccacci, S., Rossi, M., Stark, C.P., 2007. Rainfall thresholds for the initiation of landslides in central and southern Europe. *Meteorog. Atmos. Phys.* 98, 239–267.
- Guzzetti, F., Peruccacci, S., Rossi, M., Stark, C.P., 2008. The rainfall intensity-duration control of shallow landslides and debris flows: an update. *Landslides* 5, 3–17.
- Guzzetti, F., Mondini, A.C., Cardinali, M., Fiorucci, F., Santangelo, M., Chang, K.-T., 2012. Landslide inventory maps: new tools for an old problem. *Earth Sci. Rev.* 112, 42–66.
- Hastie, T., Tibshirani, R., Friedman, J., 2009. *The Elements of Statistical Learning – Data Mining, Inference, and Prediction*, second ed. Springer, New York.
- Heckmann, T., Gegg, K., Gegg, A., Becht, M., 2014. Sample size matters: investigating the effect of sample size on a logistic regression susceptibility model for debris flows. *Nat. Hazards Earth Syst. Sci.* 14, 259–278.
- Iverson, R.M., 2000. Landslide triggering by rain infiltration. *Water Resour. Res.* 36, 1897–1910.
- Knevels, R., Petschko, H., Proske, H., Leopold, P., Maraun, D., Brenning, A., 2020. Event-based Landslide modeling in the Styrian Basin, Austria: accounting for time-varying rainfall and land cover. *Geosciences* 10, 217.
- Krausse, M.K., Eastwood, C., Alexander, R.R., 2001. *Muddied Waters: Counting the National Economic Cost of Soil Erosion and Sedimentation in New Zealand*. Manaaki Whenua Press, Lincoln.
- Leonarduzzi, E., Molnar, P., McArdell, B.W., 2017. Predictive performance of rainfall thresholds for shallow landslides in Switzerland from gridded daily data. *Water Resour. Res.* 53, 6612–6625.
- Lin, Q., Steger, S., Pittore, M., Zhang, J., Wang, L., Jiang, T., Wang, Y., 2022. Evaluation of potential changes in landslide susceptibility and landslide occurrence frequency in China under climate change. *Sci. Total Environ.* 850, 158049.
- Lombardo, L., Mai, P.M., 2018. Presenting logistic regression-based landslide susceptibility results. *Eng. Geol.* 244, 14–24.
- Maraun, D., Knevels, R., Mishra, A.N., Truhetz, H., Bevacqua, E., Proske, H., Zappa, G., Brenning, A., Petschko, H., Schaffer, A., Leopold, P., Puxley, B.L., 2022. A severe landslide event in the Alpine foreland under possible future climate and land-use changes. *Commun. Earth Environ.* 3, 87.
- Marc, O., Stumpf, A., Malet, J.-P., Gosset, M., Uchida, T., Chiang, S.-H., 2018. Initial insights from a global database of rainfall-induced landslide inventories: the weak influence of slope and strong influence of total storm rainfall. *Earth Surf. Dyn.* 6, 903–922.
- Marc, O., Gosset, M., Saito, H., Uchida, T., Malet, J.-P., 2019. Spatial patterns of storm-induced landslides and their relation to rainfall anomaly maps. *Geophys. Res. Lett.* 46, 11167–11177.
- Mets, K.D., Armenteras, D., Dávalos, L.M., 2017. Spatial autocorrelation reduces model precision and predictive power in deforestation analyses. *Ecosphere* 8, e01824.
- Ministry for the Environment, 2018. *Climate Change Projections for New Zealand: Atmosphere Projections Based on Simulations from the IPCC Fifth Assessment*, second ed. New Zealand Government Ministry for the Environment, Wellington.
- Nanding, N., Rico-Ramirez, M.A., Han, D., 2015. Comparison of different radar-rain gauge rainfall merging techniques. *J. Hydroinf.* 17, 422–445.
- Neverman, A.J., Donovan, M., Smith, H.G., Ausseil, A.-G., Zammit, C., 2023. Climate change impacts on erosion and suspended sediment loads in New Zealand. *Geomorphology* 427, 108607.
- Newsome, P.F.J., Wilde, R.H., Willoughby, E.J., 2008. *Land Resource Information System Spatial Data Layers: Data Dictionary*. Landcare Research New Zealand Ltd, Palmerston North. <http://digilibRARY.landcareresearch.co.nz/cdm/ref/collection/p2002coll14/id/67>.
- Ochoa-Rodriguez, S., Wang, L.-P., Willems, P., Onof, C., 2019. A review of radar-rain gauge data merging methods and their potential for urban hydrological applications. *Water Resour. Res.* 55, 6356–6391.
- Petley, D., 2012. Global patterns of loss of life from landslides. *Geol.* 40, 927–930.
- Petschko, H., Bell, R., Leopold, P., Heiss, G., Glade, T., 2013. Landslide inventories for reliable susceptibility maps in Lower Austria. In: Margottini, C., Canuti, P., Sassa, K. (Eds.), *Landslide Science and Practice. Volume 1: Landslide Inventory and Susceptibility and Hazard Zoning*. Springer, pp. 281–286.
- Petschko, H., Brenning, A., Bell, R., Goetz, J., Glade, T., 2014. Assessing the quality of landslide susceptibility maps – case study Lower Austria. *Nat. Hazards Earth Syst. Sci.* 14, 95–118.
- Petschko, H., Bell, R., Glade, T., 2015. Effectiveness of visually analyzing LiDAR DTM derivatives for earth and debris slide inventory mapping for statistical susceptibility modeling. *Landslides* 13, 857–872.
- Phillips, C.J., Marden, M., 2005. Reforestation schemes to manage regional landslide risk. In: Glade, T., Anderson, M., Crozier, M.J. (Eds.), *Landslide Hazard and Risk*. John Wiley and Sons Ltd, Hoboken, NJ, pp. 517–547.
- Phillips, C.J., Marden, M., Basher, L.R., 2018. Geomorphology and forest management in New Zealand's erodible steeplands: an overview. *Geomorphology* 307, 107–121.
- Phillips, C., Hales, T., Smith, H., Basher, L., 2021. Shallow landslides and vegetation at the catchment scale: a perspective. *Ecol. Eng.* 173, 106436.
- Rahimi, A., Rahardjo, H., Leong, E.-C., 2011. Effect of hydraulic properties of soil on rainfall-induced slope failure. *Eng. Geol.* 114, 135–143.
- Reichenbach, P., Rossi, M., Malamud, B.D., Mihir, M., Guzzetti, F., 2018. A review of statistically-based landslide susceptibility models. *Earth Sci. Rev.* 180, 60–91.
- Reid, L.M., Page, M.J., 2002. Magnitude and frequency of landsliding in a large New Zealand catchment. *Geomorphology* 49, 71–88.
- Serrano-Notivoli, R., Tejedor, E., 2021. From rain to data: a review of the creation of monthly and daily station-based gridded precipitation datasets. *WIREs Water* 8, e1555.
- Sing, T., Sander, O., Beerenwinkel, N., Lengauer, T., 2005. ROCR: visualizing classifier performance in R. *Bioinformatics* 21, 7881.
- Smith, H.G., Spiekermann, R., Betts, H., Neverman, A.J., 2021. Comparing methods of landslide data acquisition and susceptibility modelling: examples from New Zealand. *Geomorphology* 381, 107660.
- Spiekermann, R.I., Smith, H.G., McColl, S., Burkitt, L., Fuller, I.C., 2022. Quantifying effectiveness of trees for landslide erosion control. *Geomorphology* 396, 107993.
- Steger, S., Moreno, M., Crespi, A., Zellner, P.J., Gariano, S.L., Brunetti, M.T., Melillo, M., Peruccacci, S., Marra, F., Kohrs, R., Goetz, J., Mair, V., Pittore, M., 2023. Deciphering seasonal effects of triggering and preparatory precipitation for improved shallow landslide prediction using generalized additive mixed models. *Nat. Hazards Earth Syst. Sci.* 23, 1483–1506.
- Stokes, A., Douglas, G., Fourcaud, T., Giadrossich, F., Gillies, C., Hubble, T., Kim, J., Loades, K., Mao, Z., McIvor, I., Mickovski, S., Mitchell, S., Osman, N., Phillips, C., Poesen, J., Polster, D., Preti, F., Raymond, P., Rey, F., Schwarz, M., Walker, L.R., 2014. Ecological mitigation of hillslope instability: ten key issues facing researchers and practitioners. *Plant Soil* 377, 1–23.
- Tibshirani, R., 1996. Regression Shrinkage and selection via the Lasso. *J. R. Stat. Soc. Ser. B Methodol.* 58 (1), 267–288.
- Trustrum, N.A., Gomez, B., Page, M.J., Reid, L.M., Hicks, D.M., 1999. Sediment production, storage and output: the relative role of large magnitude events in steepland catchments. *Z. für Geomorphol. Suppl.-Bd* 115, 71–86.
- Tseng, C.-W., Song, C.-E., Wang, S.-F., Chen, Y.-C., Tu, J.-Y., Yang, C.-J., Chuang, C.-W., 2020. Application of high-resolution radar rain data to the predictive analysis of landslide susceptibility under climate change in the Laonong watershed, Taiwan. *Remote Sens.* 12, 3855.
- Williams, F., McColl, S., Fuller, I., Massey, C., Smith, H.G., Neverman, A., 2022. Intersection of fluvial incision and weak geologic structures cause divergence from a universal threshold slope model of landslide occurrence. *Geomorphology* 389, 107795.

- Wilson, D.J., Western, A.W., Grayson, R.B., 2004. Identifying and quantifying sources of variability in temporal and spatial soil moisture observations. *Water Resour. Res.* 40, W02507.
- Yang, Y., Zou, H., 2015. A fast unified algorithm for computing group-lasso penalized learning problems. *Stat. Comput.* 25, 1129–1141.
- Zweifel, L., Samarin, M., Meusburger, K., Alewell, C., 2021. Investigating causal factors of shallow landslides in grassland regions of Switzerland. *Nat. Hazards Earth Syst. Sci.* 21, 3421–3437.